Check for updates

Original Article

Quantifying Biophoton Emissions From Human Cells Directly Exposed to Low-Dose Gamma Radiation

Dose-Response:
An International Journal
April-June 2020:1-7
© The Author(s) 2020
Article reuse guidelines:
sagepub.com/journals-permissions
DOI: 10.1177/1559325820926763
journals.sagepub.com/home/dos
SAGE

Jason Cohen[1], Nguyen T. K. Vo[2,3], David R. Chettle[1,3], Fiona E. McNeill[1,3], Colin B. Seymour[2], and Carmel E. Mothersill[2]

Abstract

Biophoton emission leading to bystander effects (BEs) was shown in beta-irradiated cells; however, technical challenges precluded the analysis of the biophoton role in gamma-induced BEs. The present work was to design an experimental approach to determine if, what type, and how many biophotons could be produced in gamma-irradiated cells. Photon emission was measured in HCT116 $p53^{+/+}$ cells irradiated with a total dose of 22 mGy from a cesium-137 source at a dose rate of 45 mGy/min. A single-photon detection unit was used and shielded with lead to reduce counts from stray gammas reaching the detector. Higher quantities of photon emissions were observed when the cells in a tissue culture vessel were present and being irradiated compared to a cell-free vessel. Photon emissions were captured at either 340 nm (in the ultraviolet A [UVA] range) or 610 nm. At the same cell density, radiation exposure time, and radiation dose, HCT116 $p53^{+/+}$ cells emitted 2.5 times more UVA biophotons than 610-nm biophotons. For the first time, gamma radiation was shown to induce biophoton emissions from biological cells. As cellular emissions of UVA biophotons following beta radiation lead to BEs, the involvement of cellular emissions of the same type of UVA biophotons in gamma radiation-induced BEs is highly likely.

Keywords

gamma radiation, biophoton, UVA, human, bystander effect, nontargeted effect

Introduction

The phenomenon of radiation-induced bystander effects (RIBEs) has increasingly become a topic of concern for public and environmental health. Radiation-induced bystander effects occur when nonirradiated bystander cells/organisms respond to signals released by irradiated counterparts and develop irradiated-like characteristics.[1-6] In the whole-body view, RIBEs could pose undesired damages to normal tissues following radiation therapies at the local or distant anatomical site. In the population view, RIBE signals could be transmitted from one individual to another and cause adverse effects in neighboring bystanders although beneficial/adaptive effects have also been shown.[7,8] Radiation-induced bystander effects form part of what is now widely known as the radiation-induced nontargeted effects, which predominate at the low-dose region of the radiation dose response curve. Typically, doses of less than 100 mGy and dose rates of less than 0.1 mGy/min are considered to be low according to the United Nations Scientific Committee on the Effects of Atomic Radiation.

While early RIBE research focuses on identifying the mechanisms primarily involving soluble chemical signals inducing RIBEs,[1-4,6,9,10] some evidence of possible physical signals facilitating RIBEs using rat and fish models was also reported.[11-13] Recently, our group has further shown that biophotons are emitted from beta-irradiated cells and can serve as physical signals inducing the RIBEs in bystander cells not

[1] Radiation Sciences Graduate Program, McMaster University, Hamilton, Ontario, Canada
[2] Department of Biology, McMaster University, Hamilton, Ontario, Canada
[3] Department of Physics and Astronomy, McMaster University, Hamilton, Ontario, Canada

Received 30 January 2020; received revised 21 April 2020; accepted 24 April 2020

Corresponding Author:
Nguyen T. K. Vo, McMaster University, 1280 Main Street West, Hamilton, Ontario, Canada L8S 4L8.
Email: von1@mcmaster.ca

Creative Commons Non Commercial CC BY-NC: This article is distributed under the terms of the Creative Commons Attribution-NonCommercial 4.0 License (https://creativecommons.org/licenses/by-nc/4.0/) which permits non-commercial use, reproduction and distribution of the work without further permission provided the original work is attributed as specified on the SAGE and Open Access pages (https://us.sagepub.com/en-us/nam/open-access-at-sage).

directly exposed to beta radiation.[14-17] Our group has found ultraviolet A (UVA) biophotons to be the strongest measurable signal produced by beta-irradiated cells.[14,15,17] The increasing quantities of beta radiation-induced UVA biophoton emissions were directly proportional to the increasing level of death in bystander cells.[15,17] Our radiation-induced secondary biophoton studies thus far have exclusively relied on 2 beta radiation sources, tritium and yttrium-90, that are considered pure or almost pure beta particle emitters, and both produce 100% beta yield.[14-17] This was technically important as we essentially eliminated the possibility of the photon counter to pick up gamma and stray photons that would otherwise raise the background noise and interfere with the actual UV photon counts.

Since most RIBE work uses gamma radiation, it is important to widen the studies to include gamma exposures. The important question that remains unresolved is whether gamma rays can induce biophoton emissions from irradiated biological targets. Here we report a novel experimental method that can be used to quantify biophoton emissions from gamma-irradiated cells. Our experimental method used cesium-137 (Cs-137) as the external gamma radiation source secured in a concrete casing, precise geometry of lead shielding and positioning of the photon detector and the culture flask to reduce background photon levels, and a mathematical approach to calculate the accurate emissions of biophotons from the irradiated cells. We used the human colorectal carcinoma cell line HCT116 $p53^{+/+}$ to demonstrate the proof of principle in this pilot study because this cell line is robust at producing a consistently high number of biophotons following radiation exposure.[16,17]

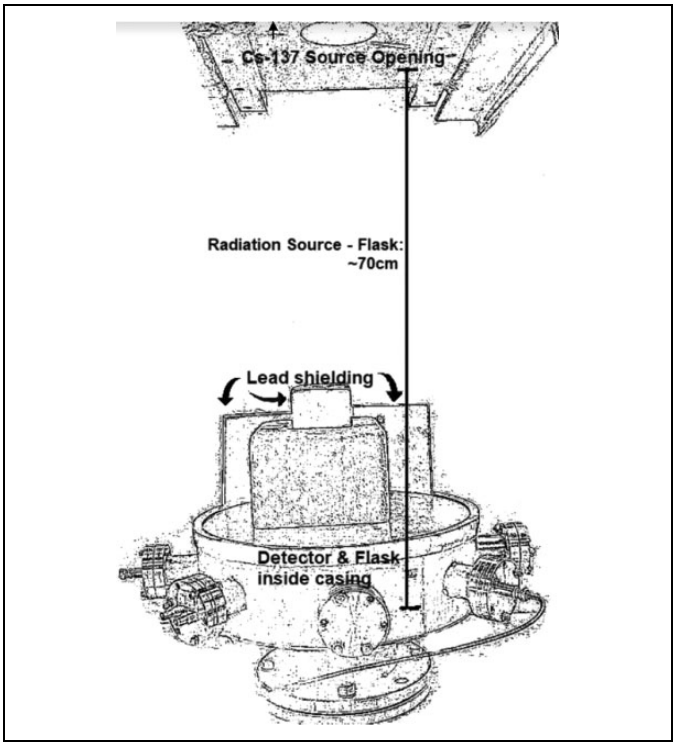

Figure 1. Schematic of radiation source to detector and flask setup. Lead shielding directly above detector was 5.5 cm in thickness, while the 2 slabs behind the detector were in total of 5.2 cm in thickness. While the lead shielding completely covered the detector, the flask (containing cells or cell-free) was exposed to the radiation source.

Materials and Methods

Cell Cultures

The human colorectal cancer cell line HCT116 $p53^{+/+}$ was cultured in the Roswell Park Memorial Institute-1640 medium supplemented with 10% fetal bovine serum, 2 mM L-glutamine, 25 mM HEPES, 100 U/mL penicillin, and 100 μg/mL streptomycin (Gibco). The cell line was grown at 37 in an atmospheric environment equilibrated at 5% CO_2 and 95% air. Subculturing was performed with trypsin/EDTA as previously described.[18] The cell line was kindly provided by Dr Shane Harding (University Health Network and University of Toronto, Toronto, Ontario, Canada).

Single Photon Counting

Photon counts were recorded using the single-photon detection unit that was designed specifically for optimally capturing photon emissions from cells cultured in tissue culture vessels.[14-17] The single photon detection unit consisted of a Hamamatsu R7400P photomultiplier tube (PMT; Hamamatsu Photonics), which was configured with a specific bandpass interference filter of choice as previously described.[14] The bandpass interference filters only allow photons at a specific wavelength to pass through. Preliminary experiments showed that the externally measurable photon signals were the most prominent at the wavelengths of 340 nm (in the UVA range) and 610 nm. Therefore, photon quantification was performed with the filter centered at 340 $\pm$ 2 nm or 610 $\pm$ 2 nm (Edmund Optics). The PMT was set to a high voltage -800 V.

Gamma-Irradiation and Photon Quantification

Two hundred fifty thousand cells were seeded in 75-cm^2 tissue culture flasks (BD Falcon) containing 15 mL of the growth medium. Control flasks had no cultured cells and contained the same volume of growth medium. After 24 hours incubation in the 37 CO_2 incubator, all flasks were brought to McMaster University's Taylor Radiobiology Suite that has Cs-137 as the gamma source. Flasks were warmed up at 37 for 10 minutes and then were gamma-irradiated for 30 seconds at room temperature (22). For every experiment, 3 photon counts were recorded concurrently with irradiation runs for background (no culture flask and no cells; accounting for stray gammas only), the cell-free control flask, and the flask with cultured cells. Net photon counts were calculated by subtracting the background counts from the flask counts. Net photon emission rates were then calculated by dividing the net photon count by 30 seconds and recoded as counts per second (cps).

The single-photon detection unit was set up 70 cm directly below the circular opening of the Cs-137 source containment

Figure 2. Positioning of the culture flask with respect to the photon detector in the single-photon counting unit. The distance between the plane of the culture flask and the detector is 6 cm.

unit (Figure 1). The detector lay within a chamber that was light tight, in order to prevent any outside light sources from affecting measurements. The detector was angled and facing downward with the detector window directly parallel to the wall of the flask that cells would anchor to (Figure 2). Directly above the detector was 5.5 cm-thick lead shielding held on top by a Styrofoam piece, and behind the detector were 2 blocks of lead shielding (totaling 5.2 cm in thickness). Because the detector was 6 cm away from the flask (Figure 2), it was arranged so that the detector would be shielded and the flask would be as exposed as possible to the direct opening of the Cs-137 source. In all experiments, irradiated flasks were approximately 70 cm away from the gamma source; at this distance, the dose rate was 45 mGy/min and 30-second irradiation yielded a total dose of 22 mGy of gamma exposure. This low dose is environmentally relevant as it is in the range of dose exposure for radioactive-exposed local animals following the aftermath of the Chernobyl and Fukushima Dai-ichi nuclear power plant meltdown accidents.[19-21]

Radiation Detection Geometry and Shielding

1. Attenuation from the shielding would still result in background coming from photons that pass through the lead (Pb), including what is called a build-up factor. The Build-up factor is the ratio of photons at a point to those that make it to the point without being scattered. When the gamma radiation reaches the Pb material, it will interact with Pb and some of the radiation will scatter or produce secondary radiation. This secondary source of radiation can make it through the shielding material, along with the less than 0.5% that did not get blocked by the shielding material. The build-up factor depends on photon energy, shielding material, and thickness of shielding material, and the build-up factors are found in the tables from Nuclear Data. For 660 keV gamma-ray photons passing through 5.5 cm of the Pb shielding material:

Without considering the build-up factor, approximately 5.5 cm of lead shielding will block >2 tenth-value layer (TVL) or about 99.5% of the initial gamma radiation. However, the buildup radiation will result in the following equation:

$$I = I_0 * b * e^{-\mu x}$$

Where I is the gamma radiation from the source that reaches the detector, I_o is the gamma radiation that is initially present before reaching the Pb shielding, b is the build-up factor for Cs-137 radiation upon Pb material, and the $e^{-\mu x}$ is the attenuating factor by which the shielding reduces the incident gamma radiation to the detector.

To calculate the build-up factor first, the number of mean free paths (mfp) is required, which is based on the mass attenuation coefficient and the density of Pb:

$$\#\,\text{mfp} = \frac{\mu}{\rho}\rho = \left(0.1102\ \text{cm}^2\text{g}^{-1}\right)\left(11.35\ \text{cm}^3\text{g}\right) = 1.25\ \text{cm}^{-1}$$
$$\mu \cdot x = \left(1.25\,\text{cm}^{-1}\right)(5.5\,\text{cm}) = 6.875$$

The mass attenuation coefficient for 662 keV gamma rays was found by National Institute of Standards and Technology.[22] The build-up factor was found by Nucleonica GmbH[23] based on the # mfp and the energy. Therefore, the build-up factor for this scenario is 3.5.

Using the tables provided by National Institute of Standards and Technology and Nucleonica GmbH,[22,23] for a point source in Pb, and interpolating for 0.661 MeV, and then interpolating for mfp = 1.25, yielded B = ~2.31. The Cs-137 radiation source was approximately 500 Ci at the time of measurements, and the detector 70 cm away from the source, resulting in the branching ratio for the 0.661 MeV gamma rays to be 0.85. The unshielded fluence rate at the time of measurements is given as:

$$\frac{500\ \cdot 3.7 \times 10^{10} \cdot 0.95}{4\ \pi\ \cdot 10^2} = 255.4\ \cdot 10^6\ \gamma \cdot \text{cm}^{-2} \cdot \text{s}^{-1}$$

Therefore, the shielded (full energy) fluence rate would be $266.8 \times 10^3\ \gamma \cdot \text{cm}^{-2} \times \text{s}^{-1}$. Scattered gamma rays can be roughly approximated to be half the energy of full energy gamma rays. The fluence rate, in terms of photon number, after the 5.5 cm Pb shield would be about 120×10^4 photons $\times$ $\text{cm}^{-2} \times \text{s}^{-1}$.

2. It must be stressed that the actual number of biophotons emitted is actually much greater than what was being detected. This is in part due to attenuation from the photons passing through the cellular material, followed by the flask, and then through the space between the emission source and the detector window. Additionally, only due to the solid angle of the detector to the plane of cells, the limited geometry of a small windowed

detector which is not all-encompassing across the cellular emissions results in most of the biophotons being undetected. The following equations represent that loss of detection due to (i) solid angle and (ii) attenuation through various media:

i) Solid angle of detector to plane of cells

$\Omega = \int\int_S \sin\theta d\theta d\varphi$. The solid angle, defined as the surface area of a sphere that is enveloped by the projection onto the sphere, or Ω, is found by integrating over the surface S across its polar (θ) and azimuthal (φ) angles. Ideally if the entire range of photons were picked up by the detector across all cells on the plane, the solid angle $\Omega = 4\pi$. However, because there is a plane (or slab) of cells which are emitting photons across all directions in a spherical geometry around them, and a detector of a small circular window that is approximately situated in the middle of the slab and 6 cm away (Figure 2), the approximate solid angle would be ~ 0.0079, which is $\sim 0.8\%$ of the entire solid angle. This means that only less than 1% of the cell luminescence observed above background is being detected by the detector. Therefore, if a detector setup existed that was able to receive 100% of the biophoton signal coming from the cells, then it would theoretically have a 100-times increase in the number of photons detected from cellular emissions.[24,25]

ii) Attenuation of biophotons due to (i) cellular material, (ii) flask material, (iii) air/space between emission source and detector window

$$\text{Incident photons} = \text{Initial photons} \times e^{-(\mu_{cell} \cdot x_1 + \mu_{flask} \cdot x_2 + \mu_{air} \cdot x_3)}$$

Where:

$\mu_{cell} = \sim 0.2\ cm^{-1}$ for 0.05 mm of tissue
$\mu_{flask} = 0.178663\ cm^{-1}$ for paraffin wax of close structure to the flask
$\mu_{air} = 0.0001039\ cm^{-1}$

x_1 = distance for biophotons to pass through the cell, or cell diameter = 0.00174 cm; x_2 = distance for biophotons to pass through thickness of flask wall = ~ 2 mm; x_3 = distance from flask wall to detector window = ~ 6 cm.[26-29]

Taking the above factors into consideration, indicating that the biophotons detected (currently seen as a significant increase above background) is still much less than the actual biophoton emission after the solid angle and attenuations limitations are realized. The following equation approximates the true number of biophotons that were theoretically present at the time of measurements:

$$I_{observed} = I_{true} \times e^{-(\mu_{cell} \cdot x_1 + \mu_{flask} \cdot x_2 + \mu_{air} \cdot x_3)} \times \Omega$$
$$I_{true} = \frac{I_{observed}}{e^{-(\mu_{cell} \times x_1 + \mu_{flask} \cdot x_2 + \mu_{air} \cdot x_3)} \times \Omega}$$

In the example of 340 nm measurements, which observed a detected biophoton count rate (above background levels) as 19 974 cps, the actual number of biophotons emitted at the time of detection was:

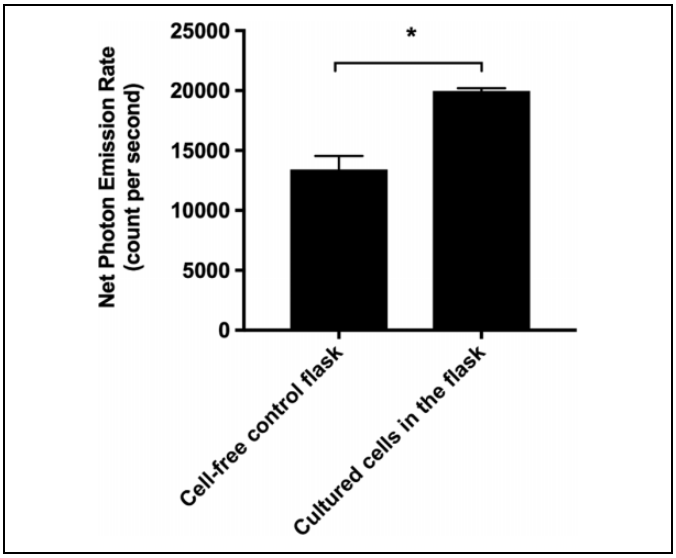

Figure 3. Net photon emission rates from culture flasks with or without 250 000 cells during a 30-second exposure to gamma irradiation with a 340 nm bandpass interference filter. A total dose of 22 mGy was administered at a dose rate of 45 mGy/min. All flasks had 15 mL of the complete growth medium. Net photon emission rates were calculated by subtracting the background count rates when there was no flask from the photon count rates when flasks were present. Data are presented as mean net photon emission rates $\pm$ SEM (n = 3). A Student *t* test with a Welch correction test was performed for statistical significance. *$P < .05$.

$$I_{true} = \frac{19.974 \times 10^3\ \text{cps}}{e^{-(\mu_{cell} \cdot x_1 + \mu_{flask} \cdot x_2 + \mu_{air} \cdot x_3)} \times 0.0079}$$
$$I_{true} = 2.623 \times 10^6\ \text{cps}$$

Therefore the true biophoton rate of emission at the time of measurement was theoretically 2 623 000 cps.

Statistical Analysis

Data are presented as mean net photon emission rates $\pm$ standard error of the mean (SEM). Student *t* tests with a Welch correction test and a 95% confidence interval were used to determine statistical significance. Value of $P < .05$ was deemed statistically significant.

Results

Emission of 340-nm (UVA) Biophotons From Gamma-Irradiated Cells

When the control flasks containing no cells were gamma irradiated, the average net photon count rate was 13415 $\pm$ 1126 cps (Figure 3), suggesting that the flask plastic materials and/or the culture medium were excited by gamma rays, releasing some UVA photons. When the flasks containing 250 000 cells were gamma irradiated, the average net photon emission rate was 19974 $\pm$ 227 cps, which was statistically significantly higher than when the cells were absent (Figure 3). Therefore,

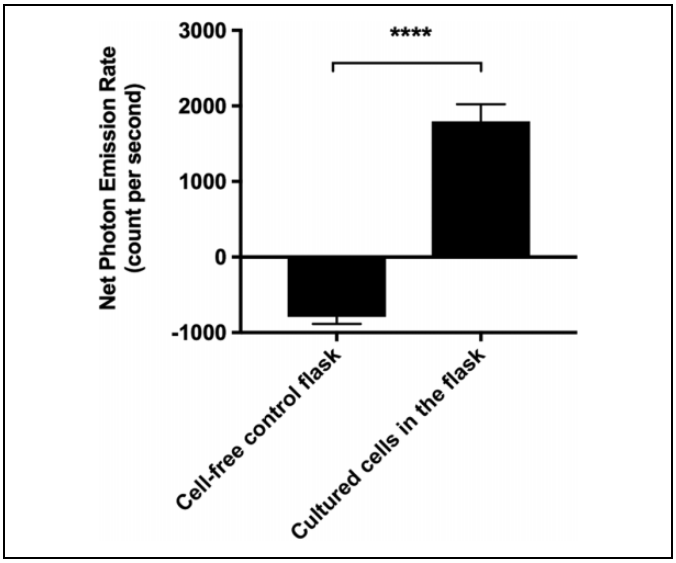

Figure 4. Net photon emission rates from culture flasks with or without 250 000 cells during a 30-second exposure to gamma irradiation with a 610 nm bandpass interference filter. A total dose of 22 mGy was administered at a dose rate of 45 mGy/min. All flasks had 15 mL of the complete growth medium. Net photon emission rates were calculated by subtracting the background count rates when there was no flask from the photon count rates when flasks were present. Data are presented as mean net photon emission rates $\pm$ SEM (n = 6). A Student *t* test with a Welch correction test was performed for statistical significance. **** $P < .0001$.

on average, 6559 $\pm$ 1148 UVA biophotons per second were emitted from 250 000 HCT116 $p53^{+/+}$ cells. As the photon detection setup could, in principle, only pick up 0.8% of the signals, the cells would have emitted 131 times higher than the recorded number, which equates to 859 229 $\pm$ 150 388 UVA biophoton emissions per second.

Emission of 610-nm Biophotons From Gamma-Irradiated Cells

When the control flasks containing no cells were gamma irradiated, the average net photon emission rate was -792 ± 92 cps (Figure 4), suggesting that the flask plastic materials and/or the culture medium absorbed some background photons from stray gammas that had energy signatures at 610 nm. When the flasks containing 250 000 cells were gamma irradiated, the average net photon emission rate was 1796 $\pm$ 226 cps, which was statistically significantly higher than when the cells were absent (Figure 4). Therefore, on average, 2588 $\pm$ 224 biophotons with 610-nm energy equivalence per second were emitted from 250 000 HCT116 $p53^{+/+}$ cells. After accounting for the 0.8% signal detection efficiency, theoretically, the cells would have emitted 339 028 $\pm$ 31 964 biophotons at 610 nm per second.

These results show that gamma radiation, even at low doses, can excite cells to emit biophotons. Additionally, the generation of UVA biophotons is significantly higher than that of 610-nm biophotons in HCT116 $p53^{+/+}$ cells. In particular, 22 mGy of gamma ray exposure led to a 2.5-fold increase in UVA biophotons as compared to 610-nm biophotons.

Discussion

The present work is the first proof of principle that gamma radiation, like beta particle radiation, also induces the emission of biophotons from biological cells. The emission or absorption of photons generated from cell-free polystyrene flasks and buffered growth media alone following radiation exposure is generally expected,[30] and that was what we also observed in the present study. Such observations are attributed to light release following atomic or molecular excitation by radiation energies.[30] Nevertheless, we observed that the net biophoton emission rate in the culture flasks containing cells was always statistically higher than that in the cell-free flasks. While naturally occurring autofluorescent events in biological cells are possible, our previous studies have shown that, with our biophoton counter, nonirradiated human cells including the HCT116 cell line do not show biophoton emissions that are above the background level.[15,17] Therefore, the data clearly show that biological cells emit biophotons following low-dose gamma radiation exposure.

Two major types of biophotons of 340-nm and 610-nm wavelengths emitted by gamma-irradiated cells were found in the present study. UVA biophotons at 340 nm make up the predominant photon energy in the UV spectral analysis following radiation from different beta emitter radioisotope sources.[14-17] In the present work, we also found a large number of UVA biophoton emissions at the same energy output (340 nm) following gamma exposure. Therefore, low-LET (linear energy transfer) ionizing radiation appears to induce cells to emit UVA biophotons. We could also detect a significantly high number of 610-nm biophotons emitted from the cells and to the best of our knowledge this is the first-ever reported emission of 610-nm biophotons by cells following radiation exposure.

Radiation-induced secondary biophotons, especially in the UVA range, have recently been shown to contribute to the RIBEs.[15-17] Secondary UVA biophotons can (1) induce direct damage in bystander cells and (2) induce bystander cells to release exosomes, which can further cause negative effects in other bystander cells.[15-17] Much of what had been learned was from studies using beta particle radiation. Our data in the present study showing that gamma rays can also induce the emission of the same type of UVA biophotons that cause RIBEs as seen in beta radiation exposure thus leads to an important implication: RIBE science is complex and RIBEs are really the consequence of the interplay of both physical and chemical signals modulating nontargeted effects that are essentially the determinants of low-dose radiation responses. In this work, 22 mGy of gamma ray exposure could induce the production rate of almost 860 000 UVA biophoton cps (approximately equivalent to 2.3×10^{-9} $Jm^{-2}s^{-1}$). In our beta radiation work, we found that the production rate of 250 UVA biophoton cps was

strong enough to cause detrimental effects on bystander cells (over the period of 7-10 days of secondary biophoton exposure).[15-17] Our work further suggests that RIBE studies must not ignore the contribution of physical signals, especially secondary UVA biophotons, to the overall RIBE outcome. We conclude that new preventive/countermeasure strategies and medical intervention approaches may need to be considered and developed to protect tissues from damages by radiation-induced secondary UV biophoton following nuclear accidents and radiotherapies.

Authors' Note

Jason Cohen and Nguyen T. K. Vo contributed equally to this work.

Acknowledgments

The authors thank Dr Shane Harding (University Health Network and University of Toronto, Toronto, Ontario, Canada) for the HCT116 cell line and Samuel Hancock (Department of Physics and Astronomy, McMaster University, Hamilton, Ontario, Canada) for his technical assistance.

Declaration of Conflicting Interests

The author(s) declared no potential conflicts of interest with respect to the research, authorship, and/or publication of this article.

Funding

The author(s) disclosed receipt of the following financial support for the research, authorship, and/or publication of this article: The authors acknowledge funding support from the Canada Research Chairs program, the Natural Sciences and Engineering Research Council (NSERC) of Canada, the National Chronic Fatigue and Immune Deficiency Syndrome Foundation, Bruce Power, and the CANDU Owners Group (COG).

ORCID iD

Nguyen T. K. Vo https://orcid.org/0000-0002-4709-3078

References

1. Azzam EI, de Toledo SM, Gooding T, Little JB. Intercellular communication is involved in the bystander regulation of gene expression in human cells exposed to very low fluences of alpha particles. *Radiat Res*. 1998;150(5):497-504. doi:10.2307/3579865
2. Azzam EI, de Toledo SM, Little JB. Direct evidence for the participation of gap junction-mediated intercellular communication in the transmission of damage signals from alpha-particle irradiated to nonirradiated cells. *Proc Natl Acad Sci U S A* 2001;98(2):473-478. doi:10.1073/pnas.011417098
3. Mothersill C, Seymour C. Medium from irradiated human epithelial cells but not human fibroblasts reduces the clonogenic survival of unirradiated cells. *Int J Radiat Biol*. 1997;71(4):421-427. doi: 10.1080/095530097144030
4. Mothersill C, Seymour CB. Cell-cell contact during gamma irradiation is not required to induce a bystander effect in normal human keratinocytes: evidence for release during irradiation of a signal controlling survival into the medium. *Radiat Res*. 1998; 149(3):256-262. doi:10.2307/3579958
5. Nagasawa H, Little JB. Induction of sister chromatid exchanges by extremely low doses of alpha-particles. *Cancer Res*. 1992; 52(22):6394-6396.
6. Narayanan PK, Goodwin EH, Lehnert BE. Alpha particles initiate biological production of superoxide anions and hydrogen peroxide in human cells. *Cancer Res*. 1997;57(18):3963-3971.
7. de Toledo SM, Asaad N, Venkatachalam P, et al. Adaptive responses to low-dose/low-dose-rate gamma rays in normal human fibroblasts: the role of growth architecture and oxidative metabolism. *Radiat Res*. 2006;166(6):849-857. doi: 10.1667/RR0640.1
8. Ryan LA, Seymour CB, Joiner MC, Mothersill CE. Radiation-induced adaptive response is not seen in cell lines showing a bystander effect but is seen in lines showing HRS/IRR response. *Int J Radiat Biol*. 2009;85(1):87-95. doi:10.1080/09553000802635062
9. Mothersill C, Bucking C, Smith RW, et al. Communication of radiation-induced stress or bystander signals between fish in vivo. *Environ Sci Technol*. 2006;40(21):6859-6864. doi:10.1021/es061099y
10. Mothersill C, Smith RW, Agnihotri N, Seymour CB. Characterization of a radiation-induced stress response communicated in vivo between zebrafish. *Environ Sci Technol*. 2007;41(9): 3382-3387. doi:10.1021/es062978n
11. Mothersill C, Moran G, McNeill F, et al. A role for bioelectric effects in the induction of bystander signals by ionizing radiation? *Dose Response*. 2007;5(3):214-229. doi:10.2203/dose-response.06-011.Mothersill
12. Mothersill C, Fernandez-Palomo C, Fazzari J, et al. Transmission of signals from rats receiving high doses of microbeam radiation to cage mates: an inter-mammal bystander effect. *Dose Response*. 2013;12(1):72-92. doi:10.2203/dose-response.13-011.Mothersill
13. Mothersill C, Smith RW, Fazzari J, McNeill F, Prestwich W, Seymour CB. Evidence for a physical component to the radiation-induced bystander effect? *Int J Radiat Biol*. 2012; 88(8):583-591. doi:10.3109/09553002.2012.698366
14. Ahmad SB, McNeill FE, Byun SH, et al. Ultra-violet light emission from HPV-G cells irradiated with low let radiation from (90)Y; consequences for radiation induced bystander effects. *Dose Response*. 2013;11(4):498-516. doi:10.2203/dose-response.12-048.Ahmad
15. Le M, McNeill FE, Seymour C, Rainbow AJ, Mothersill CE. An observed effect of ultraviolet radiation emitted from beta-irradiated HaCaT cells upon non-beta-irradiated bystander cells. *Radiat Res*. 2015;183(3):279-290. doi:10.1667/RR13827.1
16. Le M, Fernandez-Palomo C, McNeill FE, Seymour CB, Rainbow AJ, Mothersill CE. Exosomes are released by bystander cells exposed to radiation-induced biophoton signals: reconciling the mechanisms mediating the bystander effect. *PLoS One* 2017; 12(3):e0173685. doi:10.1371/journal.pone.0173685
17. Le M, Mothersill CE, Seymour CB, Rainbow AJ, McNeill FE. An observed effect of p53 status on the bystander response to radiation-induced cellular photon emission. *Radiat Res*. 2017; 187(2):169-185. doi:10.1667/RR14342.1
18. Vo NTK, Sokeechand BSH, Seymour CB, Mothersill CE. Influence of chronic low-dose/dose-rate high-LET irradiation from

radium-226 in a human colorectal carcinoma cell line. *Environ Res*. 2017;156(5):697-704. doi:10.1016/j.envres.2017.04.041

19. Hancock S, Vo NTK, Byun SH, Zainullin VG, Seymour CB, Mothersill C. Effects of historic radiation dose on the frequency of sex-linked recessive lethals in Drosophila populations following the Chernobyl nuclear accident. *Environ Res*. 2019;172: 333-337. doi:10.1016/j.envres.2019.02.014
20. Hancock S, Vo NTK, Omar-Nazir L, et al. Transgenerational effects of historic radiation dose in pale grass blue butterflies around Fukushima following the Fukushima Dai-ichi Nuclear Power Plant meltdown accident. *Environ Res*. 2019;168(1): 230-240. doi:10.1016/j.envres.2018.09.039
21. Hancock S, Vo NTK, Goncharova RI, Seymour CB, Byun SH, Mothersill CE. One-Decade-Spanning transgenerational effects of historic radiation dose in wild populations of bank voles exposed to radioactive contamination following the chernobyl nuclear disaster. *Environ Res*. 2020;180(4):108816. doi:10. 1016/j.envres.2019.108816
22. National Institute of Standards and Technology. X-ray mass attenuation coefficients. (2009). Accessed August 1, 2019. https://physics.nist.gov/PhysRefData/XrayMassCoef/ElemTab/z82.html
23. Nucleonica GmbH. Dosimetry & shielding H*(10). 2020. Accessed May 5, 2020. https://www.nucleonica.com/wiki/index.php?title=Help:Dosimetry_%26_Shielding_H*(10)#Build-up_Factors_.28B.29_for_Shield_Materials
24. Nestor's Microscopy & Microanalysis Tool Set. 2013. Accessed August 1, 2019. http://tpm.amc.anl.gov/NJZTools/XEDSSolidAngle.html
25. Nestor's Microscopy & Microanalysis Tool Set. 2013. Accessed August 1, 2019. http://tpm.amc.anl.gov/NJZTools/Zaluzec-Preview-SolidAngleFormulaePaper.pdf
26. Tahara M, Inoue T, Sato F, et al. The use of Olaparib (AZD2281) potentiates SN-38 cytotoxicity in colon cancer cells by indirect inhibition of Rad51-mediated repair of DNA double-strand breaks. *Mol Cancer Ther*. 2014;13(5):1170-1180. doi:10.1158/1535-7163.MCT-13-0683
27. Chen A, Luo J, Wan A. Fat to muscle ratio measurements with dual energy X-ray absorbtiometry. *Nucl Instrum Methods Phys Res. A* 2015;788(1):24-28.
28. Risk Assessment Information System. Lin coefficients. 2019. Accessed August 1, 2019. https://rais.ornl.gov/tools/Lin_Coefficients.pdf
29. Mousa A, Kusminarto K, Suparta GB. A new simple method to measure the X-ray linear attenuation coefficients of materials using micro-digital radiography machine. *Int J Applied Eng Res*. 2017;12(21):10589-10594.
30. Ahmad SB, McNeill FE, Byun SH, Prestwich WV, Seymour C, Mothersill CE. Ion beam induced luminescence; relevance to radiation induced bystander effects. *Nucl Instrum Methods Phys Res. B*. 2012;88:81-88. doi:10.1016/j.nimb.2012.05.043